Morphology Development and Dynamics of Photopolymerization-Induced Phase Separation in Mixtures of a Nematic Liquid Crystal and Photocuratives

Domasius Nwabunma, Hao-Wen Chiu,† and Thein Kyu*

Institute of Polymer Engineering, The University of Akron, Akron, Ohio 44325

Received July 26, 1999; Revised Manuscript Received November 12, 1999

ABSTRACT: Dynamics of photopolymerization-induced phase separation (PIPS) and morphology development in mixtures of low molar mass nematic liquid crystal (LC) 4-*n*-heptyl-4′-cyanobiphenyl (designated K21) and photocuratives (designated NOA65) have been investigated by means of optical microscopy, light scattering, and differential scanning calorimetry. The equilibrium phase diagram of the LC/monomer (uncured NOA65) system was first established theoretically on the basis of the Flory−Huggins/Maier−Saupe theory. The calculated phase diagram displayed isotropic, liquid + liquid, liquid + nematic, and pure nematic coexistence regions in conformity with experiment. The effect of photopolymerization on the phase diagram was examined through comparison of the calculated phase diagrams of LC/linear polymer with LC/cross-linked polymer mixtures. Photopolymerization of the LC/monomer mixtures resulted in phase separation due to instability caused by an increase in molecular weight and subsequent network formation. Photopolymerization initiated in the isotropic phase gave uniformly distributed polygonal-shaped LC droplets in contrast to photopolymerization initiated in the two-phase region. Of particular interest is that the size of the phase-separated LC droplet increases with LC concentration. The network morphology is reminiscent of an interconnected thread seemingly running through the interstices of the polygonal droplets. Temporal evolution of structure factors was analyzed in the context of dynamical scaling law.

Introduction

Inhomogeneous thin films composed of low molar mass liquid crystal (LC) and polymer are potential materials for various electrooptical devices such as optical switches (light shutters), variable transmittance (transparency) windows, and reflective displays. Typical examples include polymer-dispersed liquid crystals (PDLC)[1−3] containing a substantial amount of polymer and polymer-stabilized liquid crystals (PSLC)[4] containing very little polymer in the form of a network. The polymer matrix basically provides thermal and mechanical stability, while the LC affords needed electrooptical properties. The anisotropic optical properties of these composites may be exploited by electrically switching them between a strong scattering "off" state and an optically transparent "on" state. PSLC are preferred to PDLC since the former possesses fast electrooptical responses close to those of the neat LC. Furthermore, incorporation of a chiral agent or cholesteric LC in PSLC would be useful for reflective color displays.[4] PDLC composites hitherto reported typically involve flexible chain polymers and liquid crystals. The liquid crystal may be nematic,[5−8,13] cholesteric,[9−12] or a fast switching smectic C* (ferroelectrics).[14−23] Recently composites containing liquid crystalline polymers as the matrix have been studied.[24−26]

Photopolymerization-induced phase separation is a preferred way of making LC/polymer network composites because the fabrication process is simple, fast, clean, and solvent-free. Polymerization at a low temperature minimizes degradation and/or loss of LC, monomer, or photoinitiator via evaporation. A proper choice of temperature and polymerization rate further allows for better control of morphology.[8,10,11,13] In addition, the use of laser photopolymerization enables the production of modulated or target structures. Photopolymerization has thus found applications not only in the making of LC/polymer composites but also in diverse applications such as polymer/polymer composites, coatings, adhesives, photolithography, and dental restorative materials.

It is well established that the morphology strongly affects the electrooptical properties of LC/polymer composites.[2,4,5,8,11,19,25,27−29] In general, the morphology is controlled by the relative rates of reaction and of phase separation, which depends on a number of factors such as type of LC and monomer, LC concentration, monomer functionality, irradiation intensity and time, and polymerization temperature. Another important, but often neglected, factor is the polymerization environment. Photopolymerization initiated in the isotropic or the two-phase coexistence region can exert a profound influence on the emergence of morphology.[30] Thus, it is essential to establish the phase diagram of the LC/monomer system before attempting any study on the dynamics of polymerization-induced phase separation (PIPS).

In previous studies,[30,31] we have examined the influence of the LC/monomer phase behavior on the photopolymerization kinetics of a mixture of nematic LC, 4-*n*-heptyl-4′-cyanobiphenyl (designated K21), and photocurable multifunctional thiolene-based optical adhesive (designated NOA65). In the present study, we investigate the morphology development and phase separation dynamics during photopolymerization. Using the starting LC/monomer phase diagram as a guide for photopolymerization, the effects of temperature and LC concentration on the emergence of the domain morphol-

† Present address: Gentex Optics, R & D Materials Division, Dudley, MA 01571.

* Corresponding author: e-mail tkyu@uakron.edu.

10.1021/ma9912296 CCC: $19.00
Published on Web 01/13/2000

ogy of the composites (LC + polymer network) have been examined. The morphology of the polymer network is also investigated by means of scanning electron microscopy (SEM) after removal of the LC using appropriate solvent. Finally, the mechanism of photopolymerization-induced phase separation and structure formation is elucidated on the basis of the temporal evolution of morphology and structure factors.

Experimental Section

Materials and Procedures. The photopolymerizable thiolene-based optical adhesive (NOA65) was purchased from Norland Products Inc. NOA65 is premixed with 5 wt % benzophenone photoinitiator.[32] It has an optical absorption in the 350−380 nm range with a density[33] of 1.12 g/cm^3 and an weight-average molecular weight[32] of 400 g/mol. The liquid crystal used was a single-component nematic, i.e., 4-*n*-heptyl-4′-cyanobiphenyl (K21) purchased from BDH Chemicals. K21 exhibits a crystal to nematic transition temperature (T_{KN}) at 28.5 °C and a nematic to isotropic transition temperature (T_{NI}) at 42 °C. NOA65 and K21 were used as received.

Regarding the establishment of the phase diagram and the investigation of morphology development and phase separation dynamics, several LC/monomer mixtures were prepared by weighing desired amounts of NOA65 and K21 in small vials and then mixed by stirring vigorously using a magnetic stirrer. The liquid mixtures were stored in a refrigerator and handled under dimmed light to minimize photopolymerization.

Phase Diagram of Starting LC/Monomer Mixtures. For the optical microscopy experiment, a Nikon Optipot 2-POL microscope with a filtered halogen light source (12 V, 100 W) was used with a magnification of 400×. A sample hot stage (Linkam Scientific Instruments, model TS1500) interlinked to a programmable temperature controller (Linkam, model TMS93) and a cooling system (model LNP93/2) was used. Samples were covered with glass slides, then heated until they were optically isotropic, and then cooled slowly. The temperature of phase change was monitored under the optical microscope. Thereafter, the samples were reheated to their isotropic states. The experiment was repeated to ensure reproducibility. The heating and cooling rate was 1 °C/min.

In the light scattering experiment, a 2 mW randomly polarized He−Ne laser light source (Aerotech, model LSR2R) with a wavelength of 632.8 nm was utilized. Cloud points were measured by monitoring the scattered intensity at a fixed angle (∼10°) using a photodiode detector (Hamamatsu Co., model HC-220-01). A sample hot stage coupled with a programmable temperature controller (Omega, model CN-2012) having a resolution of ±0.1 °C was utilized for temperature scans at the rate of 1 °C/min. A personal computer and an A/D converter were linked to the light scattering equipment for data acquisition and analysis.

For the differential scanning calorimetry (DSC) experiment, a Du Pont thermal analyzer (model 9900) equipped with a heating module (model 910) was used under nitrogen circulation. Liquid nitrogen was used as a purging and cooling medium. The heating rate was 5 °C/min. Samples in the recommended amount of 10−15 mg by weight were sealed in hermetic pans. DSC scans were undertaken in the temperature range 0−50 °C to determine the nematic−isotropic transitions of the neat K21 and of its mixtures.

Preparation of LC/Photo-Cross-Linked Polymer Composites. K21/uncured NOA65 mixtures of various compositions were sandwiched between two microscope glass slides with spacers to yield a thickness range of 10−20 μm. These samples were photopolymerized isothermally under the optical microscope at 20 and 40 °C corresponding to the two-phase and the isotropic single phase of these blends, respectively.

The photo-cross-linking was done under either continuous or intermittent irradiation using a curing unit (Electrolite Corp., model ELC403) equipped with a UV guide tip capable of swiveling 360°. The UV intensity output of the lamp was 40 mW in the 340−380 nm range. The distance between the UV guide tip and the sample was about 30 mm, and the illuminated area was 1 cm^2. Thin samples were used to minimize the effect of thickness on the absorbed radiation and the emerging structures. Also, the sample area exposed to the radiation was kept sufficiently small to ensure uniform radiation over the entire sample. Prior to photopolymerization at a desired temperature, the samples were preheated to the isotropic region to ensure uniformity in thickness and thermal history.

Examination of Morphology of LC/Polymer Network Composites. Morphological pictures were acquired under polarized and unpolarized light by means of a Nikon optical microscope equipped with a Nikon FX-35DX camera and a Nikon UFX-DX exposure controller. The emerging morphology was examined as a function of temperature, LC concentration, and irradiation time.

To examine the polymer network morphology, the glass slide containing the LC/polymer composite was immersed in *n*-heptane for 2 days and washed several times to extract the LC while leaving the polymer network domains intact, as the polymer network can no longer be dissolved in *n*-heptane. The glass slide containing the network was cut to an appropriate size to fit the geometry of the scanning electron microscope (SEM) sample holder. The specimen was then sputtered with silver under argon gas using a sputter-coating device (Polaron, model ISI-5400). The morphology of the network was then examined using Hitachi Corp. SEM (model S-2150).

Investigation of Time Evolution of Morphology and Phase Separation Dynamics. To mimic the dynamics of phase separation and structure development, optical images of the phase-separated structures were captured at different irradiation or exposure times using a Snappy digital image acquisition board (Connectivity Inc.). Structural analysis was then performed on the acquired images by taking a two-dimensional fast Fourier transform (2D-FFT). It should be noted that 2D-FFT of phase-separated structures was taken since the phase separation dynamics could not be followed in real time using the conventional time-resolved light scattering equipment due to interference from the UV radiation with He−Ne laser light and the charge coupled detector (CCD). 2D-FFT provided the scattering patterns and structure factors, S, as functions of irradiation time, t, and wavenumber, q. The change of q_{max} with t was analyzed in the context of the familiar power law relationship of the form $q_{max} = t^{-\alpha}$, where α is the scaling exponent.

Results and Discussion

Phase Diagram of LC/Monomer System before Photopolymerization. Figure 1 shows the experimental phase diagram as obtained by light scattering, optical microscopy, and DSC in comparison to theory (solid line). The theoretical calculation for the coexistence line was carried out on the basis of the combined Flory−Huggins[36,37] (FH)/Maier−Saupe[38] (MS) theory and was plotted against the volume fraction of the liquid crystal, φ_L. The LC/monomer phase diagram is of the upper critical solution temperature (UCST) type overlapping with the nematic−isotropic transition of the LC. This phase diagram is thermally reversible and similar to that of nematic/linear polymer mixtures.[34,39−47] The predicted LC/monomer phase diagram displays various coexistence regions such as liquid + liquid (I + I), nematic + liquid (N + I), and pure nematic phases (N). Below the peritectic line (dotted horizontal line), liquid and nematic phases coexist. By monitoring the phase separation (emerging LC domains) and concomitant nematic ordering using optical microscopy, the coexistence regions may be identified.

Upon cooling the 90/10 mixture from an isotropic phase (35 °C) to a two-phase region, birefringent droplets appear around 24 °C, suggestive of nematic (N)

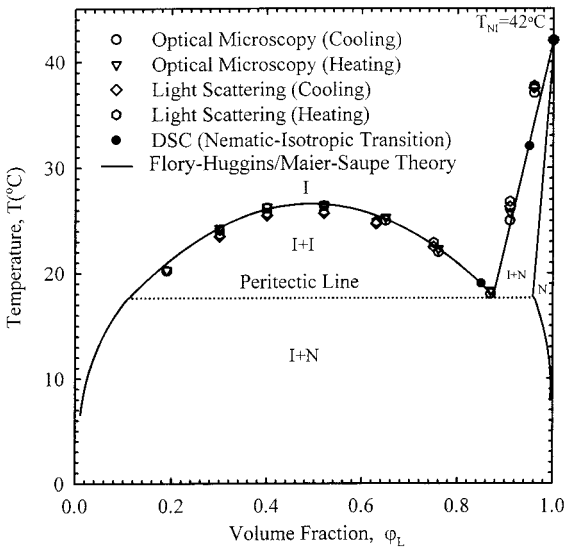

Figure 1. Phase diagram of K21/NOA65 monomer system before photopolymerization as obtained using optical microscopy, light scattering, and DSC. The solid line denotes the theoretical curve calculated based on the combined Flory−Huggins (F−H)/Maier−Saupe (M−S) theory. The symbol φ_L represents the volume fraction of the liquid crystal.

+ isotropic liquid (I) phase separation (Figure 2a). It is apparent from the LC/monomer phase diagram that there is no liquid + liquid coexistence region in the mixtures of high LC content mixtures (see Figure 1). The LC droplets grow in time via coalescence, while exhibiting a Schlieren texture (under crossed polarizers), which is a typical feature of nematics. Similarly, isotropic liquid + isotropic liquid (I + I) phase separation first occurs in the 60/40 mixture around 24 °C (Figure 2b). The existence of the I + I region at the 60/40 composition is consistent with the LC/monomer phase diagram (see Figure 1). The droplets are isotropic initially. With the progression of time, the average size increases as the LC fraction increases. Nematic textures develop subsequently around 14 °C. It is apparent from Figure 2a,b that the emerged morphology such as texture, size, and distribution of LC droplets depends on the composition and the coexistence regions.

Effect of Polymerization (Linear versus Cross-Linking) on Phase Diagram. When the LC/monomer mixture is polymerized in the isotropic phase, the mixture becomes unstable and undergoes phase separation due to thermodynamic instabilities induced by the increase in molecular weight of the growing polymer. Subsequently, the LC/polymer coexistence curve moves upward to a higher temperature, while shifting toward the LC-rich region in a manner dependent on the extent of reaction (or conversion). Since the polymerizable material (NOA65) is multifunctional, it is likely that the growing polymer undergoes cross-linking. The molecular weight between the cross-linked points decreases, which further drives the instability of the system. In this regard, the free energy arising from the network elasticity becomes important in the description of thermodynamic phase equilibria.

Figure 3 depicts the calculated phase diagrams of blends of LC/linear polymer and LC/cross-linked networks. Also included in Figure 3 is the phase diagram of the starting LC/monomer mixture as a reference. Note that the labeled coexistence regions for the LC/linear polymer and LC/cross-linked systems have been

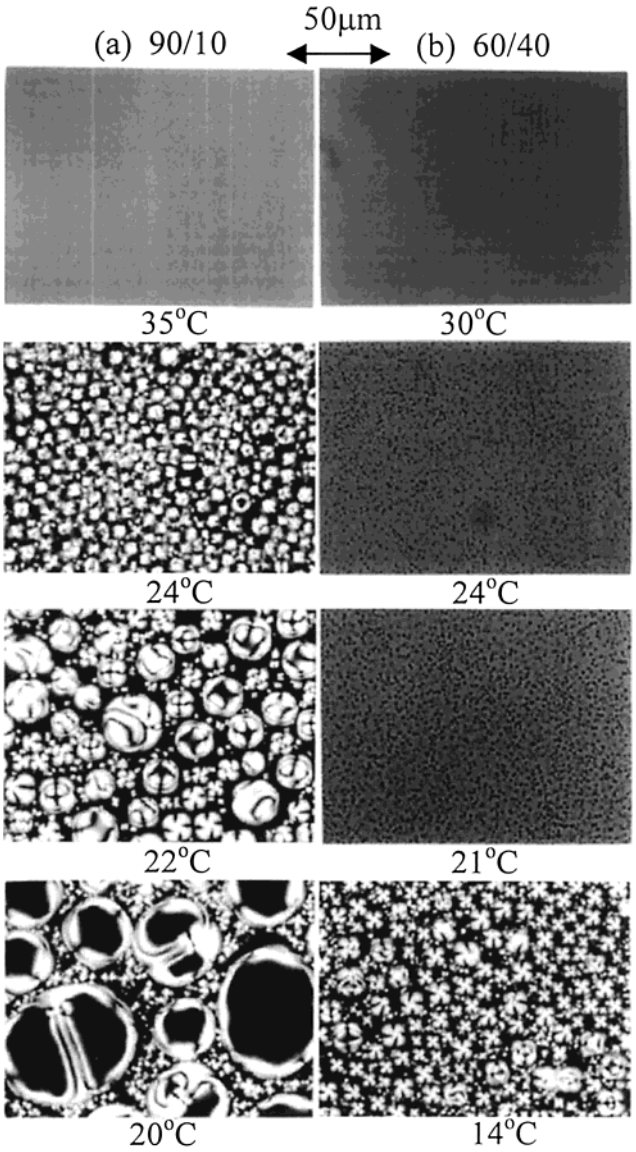

Figure 2. Morphological changes observed during cooling (without photopolymerization) of (a) the 90/10 K21/NOA65 mixture showing isotropic liquid (35 °C) to liquid + nematic coexistence regions (<24 °C) and (b) the 60/40 mixture showing isotropic liquid (30 °C), isotropic liquid + isotropic liquid (24−21 °C), and isotropic liquid + nematic coexistence phases (14 °C). The cooling rate was 1 °C/min.

italicized to distinguish them from those of the LC/monomer system. For the purpose of comparison, the statistical segment length (r_p) of the linear polymer, and that between cross-links (r_c) of the cross-linked polymer, were simply taken as 100. The detailed calculations on the effect of molecular weight, network functionality, etc., on the phase diagram topology may be found in our earlier paper.[31] As depicted in Figure 3, the coexistence curve moves upward to a higher temperature and asymmetrically to a higher LC side during photopolymerization.

As polymerization advances the segment length of linear polymer, r_P increases, which drives the binodal curve to move upward. When the coexistence curve surpasses the reaction temperature (indicated by the point x in Figure 3), phase separation occurs. The LC/linear polymer blends segregate eventually into the LC-rich and LC-poor phases. However, the moment the cross-linking reaction commences, the segment length

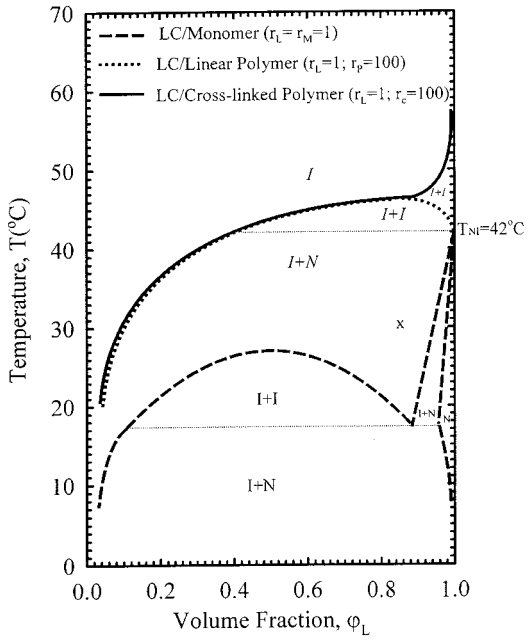

Figure 3. Calculated phase diagrams for LC/linear polymer (dotted line) and LC/cross-linked polymer systems (solid line) along with that of the LC/starting monomer mixture (dashed line) as a reference. Note that the labeled coexistence regions for the LC/linear polymer and LC/cross-linked polymer systems have been italicized to distinguish them from those of the LC/monomer system. As in Figure 1, the symbol φ_L represents the volume fraction of the liquid crystal.

between the cross-linked points, r_c, decreases. In both events, the emerging polymer becomes less soluble in the LC solvent. The binodal curve shifts asymptotically toward the high LC volume fraction axis with the progression of the cross-linking reaction. Unlike the LC/linear polymer system, there is no identifiable critical point in the LC/cross-linked polymer phase diagram. Instead, the coexistence curve makes an upward turn asymptotically near the pure LC axis. The observed difference in the phase diagram topologies, particularly the I + I coexistence regions, may be attributed to the network formation. Below the NI transition temperatures of the LC, nematic is formed in the LC-rich phase, giving rise to the coexistence of isotropic liquid (I) + nematic (N) region. The I + N coexistence envelope widens with the progression of both linear and cross-linking polymerization.[31]

Morphology of LC/Network Composites after Photopolymerization. Effect of Temperature and Concentration. To examine the emerging morphology as a function of temperature, photopolymerization was performed on three different mixtures of high LC concentrations (85%, 90%, and 95%). Figure 4a shows optical micrographs of the morphology observed under crossed and uncrossed polarizers after photopolymerization of 85/15, 90/10, and 95/5 K21/NOA65 blends in the two-phase (I +N) region at 20 °C. A heterogeneous texture with unevenly distributed LC droplets can be discerned. If these blends were to be used for display or control devices, the LC orientation in the smaller domains would obviously respond differently to an applied electric field from that of the larger LC domains. The nonuniformity in the LC droplet sizes would thus result in inferior electrooptical switching performance.

Figures 4b, on the other hand, shows the optical micrographs of morphology of the 85/15, 90/10, and 95/5 K21/NOA65 mixtures subjected to photopolymerization

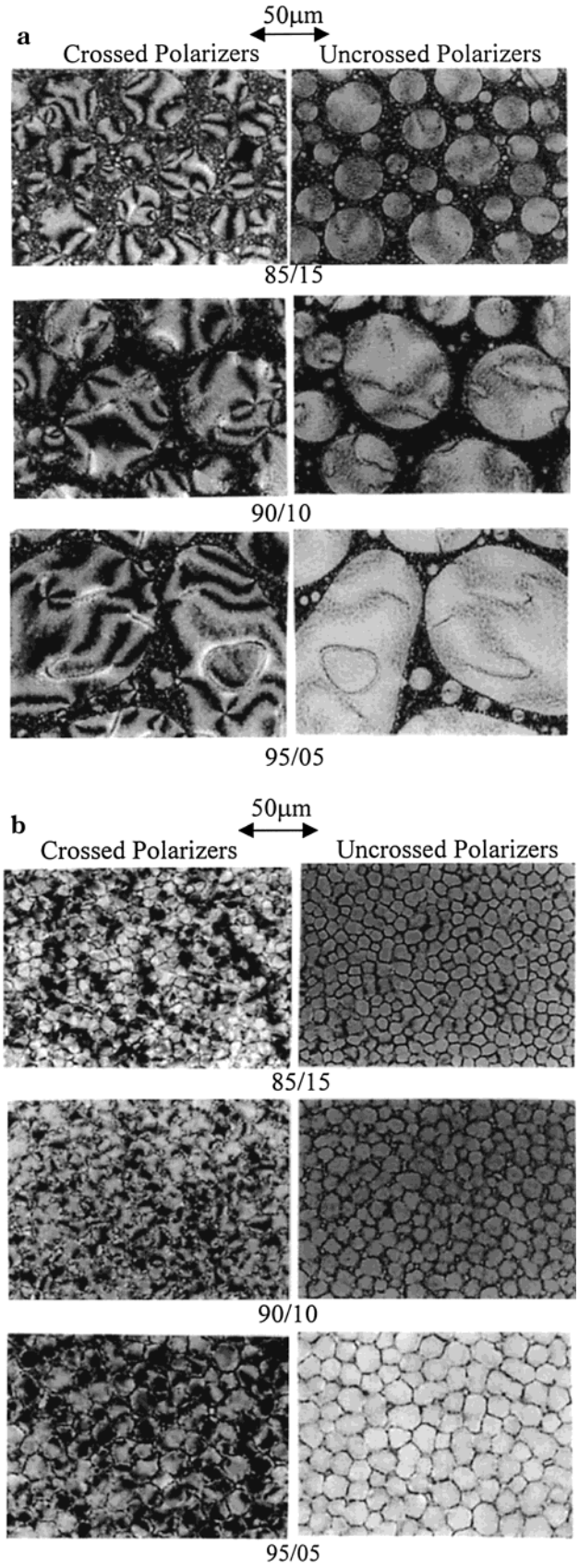

Figure 4. Optical micrographs under crossed polarizers and unpolarized light for the 85/15, 90/10, and 95/5 K21/NOA65 mixtures showing the dependence of domain size on LC concentration after photopolymerization (a) in the two-phase region (20 °C) and (b) in the isotropic phase (40 °C) for 300 s, with UV intensity of the lamp of 40 mW and the illumination area of 1 cm^2.

in the isotropic region at 40 °C, showing a uniformly distributed LC droplet morphology having a polygonal shape in the 85/15 composition. It should be noted that the observed morphology is a 2-dimensional representation of 3-dimensional droplets. Serbutoviez et al.[13] made a similar observation in nematic LC/photocross-linked diacrylate systems. Using confocal microscopy, Amundson and co-workers[48] observed a similar "polyhedral foam texture" and claimed that it is quite distinct from the "Swiss cheese" morphology where the LC droplets are well separated by the polymer matrix and are more spherical in shape. In view of the uniformity of the droplets in the latter case, we shall focus on the emergence of the evenly distributed nonspherical droplet morphology.

The observed morphology of photopolymerized 90/10 and 95/5 mixtures, also depicted in Figures 4b, is apparently similar to that of the 85/15 mixture. A closer examination of the morphology of 90/10 and 95/5 mixtures reveals that as the LC fraction in the initial mixture increases so does the size of the phase-separated LC droplets, which is consistent with the experimental observation of Amundson et al.[48] This observation is not surprising in view of the fact that with increasing LC concentration more LC molecules are expected to segregate out from the polymer network. The observed influence of the LC concentration on the droplet size and its distribution may be important for the improvement of electrooptical properties.

Polymer Network Morphology. It is of interest to examine the morphology of the polymer network after the extraction of the LC from the composite. Figure 5 shows the optical microscopy (top image) and the SEM (lower image) observations of the network morphology observed for the 95/5 K21/NOA65 mixture. The polymer network seemingly runs through the interstices of the polygonal domains. The threadlike morphology can be discerned more clearly in the SEM micrograph. In the literature, network morphologies such as beadlike, fiberlike, platelike, and helicoidal have all been observed[4,10,11,49] in LC/polymer network mixtures. These LC materials were either nematic or cholesteric, while the networks were made of rigid mesogens or flexible multifunctional reactive monomers.

Rajaram et al.[10,11] found that the morphology of nonmesogenic BAB diacrylate network after photopolymerization in nematic liquid crystal 5CB and eutectic nematic liquid crystal (E48) was beadlike in both nematic and isotropic states of these two liquid crystals. In the case of nonmesogenic BAB-6 diacrylate, photopolymerization in 5CB resulted in a fiberlike morphology if 5CB were in the nematic state,[10] but it resulted in beadlike when 5CB was in the isotropic state.[10] However, the photopolymerization of BAB-6 in E48 gave a fiberlike appearance if E48 was in either the nematic or the isotropic state.[11] Furthermore, Rajaram et al.[11] further reported that the morphology of mesogenic BABB-6 diacrylate network after photopolymerization in E48 appeared fiberlike if E48 was in the nematic state and platelike if E48 was in the isotropic state. In the work of Rajaram et al.,[10,11] the polymerization took place in either homogeneous or homeotropic states of the LC. On the other hand, Yang et al.[4] and Chien et al.[49] found a helicoidal morphology for the BABB-6 network after photopolymerization in the planar texture of the cholesteric LC (E48 + chiral dopant 15CB).

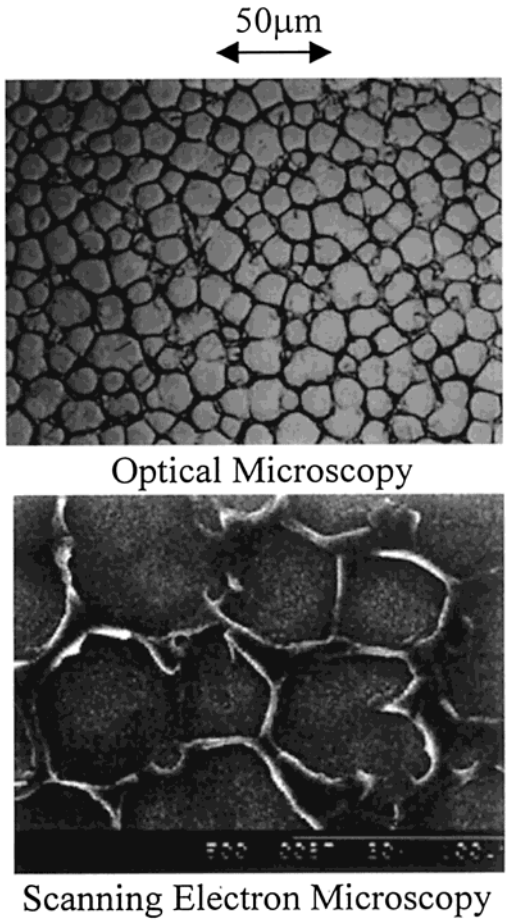

Figure 5. Optical (upper) and SEM (lower) micrographs showing the interconnected morphology observed after photopolymerization of the 95/5 K21/NOA65 mixture at 40 °C for 300 s and with UV intensity of 40 mW/cm^2. The LC/monomer mixture before polymerization was initially in the isotropic phase at 40 °C. The scale bar of the SEM micrograph is 100 μm.

As reported earlier,[4,10,11,49] the network morphology obtained depends on many factors such as structure, concentration, and functionality of reactive monomers and LC, as well as photopolymerization conditions such as temperature, UV intensity, irradiation time, and homogeneous or homeotropic preorientated states. Judging from the observed domain morphologies, it seems as though there is no unique criterion in obtaining a given network morphology. It should be emphasized that these emerging morphologies are nonequilibrium in nature, and thus it is necessary to understand the dynamics of photopolymerization-induced phase separation.

Dynamics of Photopolymerization-Induced Phase Separation. Experimental studies on phase separation dynamics in thermal-quenched[40,41,46,50−52] and in thermal-initiated polymerizing[53,54] mixtures containing liquid crystals are well documented. Such studies usually involve the combination of morphology evolution and radiation scattering to elucidate the mechanism of phase separation. Regarding photopolymerization-induced phase separation, very few real time studies exist for LC/polymer systems.[13,55] According to Serbutoviez et al.,[13] photopolymerization-induced liquid−gel phase separation occurs in a LC/photo-cross-linked network mixtures via the nucleation and growth mechanism. However, Srinivasarao et al.[55] found that

spinodal decomposition is the mechanism that is responsible for PIPS. Although the two studies are encouraging, the opposing views have yet to be reconciled.

In general, it is difficult to probe the dynamics of photopolymerization-induced phase separation in real time using the conventional time-resolved light scattering because of the strong interference of the UV radiation with the scattered light. To circumvent this interference problem, the UV light may be turned off intermittently during acquisition of CCD images of the emerging patterns during the optical microscopic investigation. There is a natural concern that intermittent illumination of the UV radiation might affect the domain growth in PIPS. To alleviate the aforementioned problem, photopolymerization was carried out in two different ways. In the first approach, UV light was illuminated intermittently on a single specimen; that is, the UV light was turned off during image acquisition and then immediately switched on again. The time for capturing one CCD image frame was less than 1 s. In the second method, a fresh specimen was utilized each time and continuously exposed to UV light for a chosen time, after which the morphology was examined. As depicted in Figure 6, visual inspection of the morphology obtained from the two methods revealed that the domain size and its distribution appear comparable. This gives us some optimism, although it is by no means ideal, to use the intermittent illumination approach in the examination of the dynamics of phase separation and morphology development subjected to photopolymerization.

We restricted our phase separation dynamics experiment to photoinitiation in the isotropic phase as it affords LC/polymer composites with more uniform morphology. In addition, 2-dimensional Fourier transformation was performed on the observed structures to obtain the scattering patterns and to analyze the mechanism of structure formation and growth dynamics based on the temporal evolution of the structure factors. Figure 7 depicts the time evolution of morphology (first column) and the corresponding scattering patterns (second column) obtained during photopolymerization at 40 °C for the 95/5 K21/NOA65 blend. As shown in Figure 7, phase separation was detected under the microscope within 15 s of UV exposure. The 95/5 mixture being in the nematic-rich region, the droplet morphology emerges and appears uniform. It is difficult to assign any particular mechanism (e.g., nucleation and growth or spinodal) on the basis of the optical microscopic images alone. The corresponding scattering halo from the 2D-FFT suggests that the phase separation process presumably occurs through spinodal, but it has already advanced to the intermediate and late stages where these droplets grow quickly with time through coalescence. The coarsening process is particularly pronounced in the 95/5 K21/NOA65 blend because of the high mobility of the LC molecules. When the cross-linking reaction starts, a polymer network is formed in the polymer-rich region (interstices of LC droplets). The formation of polymer networks presumably impedes the growth of these droplets, thereby virtually ceasing the growth. As a consequence, these droplets impinge on each other, resulting in a change of the domain topology from a spherical to a polygonal shape.

The 50/50 mixture seemingly corresponds to the critical composition of the UCST before the photopolymerization (Figure 1). However, with the progression of reaction, the UCST maximum not only moves to a higher temperature but also shifts asymmetrically to the higher LC volume fraction (Figure 3). When the coexistence curve surpasses the reaction temperature, phase separation occurs and the 50/50 blend is no longer the critical point. Hence, the reaction temperature must cross the metastable region where the nucleation and growth are prevalent. As depicted in Figure 8 (column A), the domains appear interconnected. However, they are too small to be distinguished from the droplets (as droplet morphology could appear interconnected in the 2-D projection of 3-D objects on the optical plane). The corresponding scattering halo (not shown) suggestive of

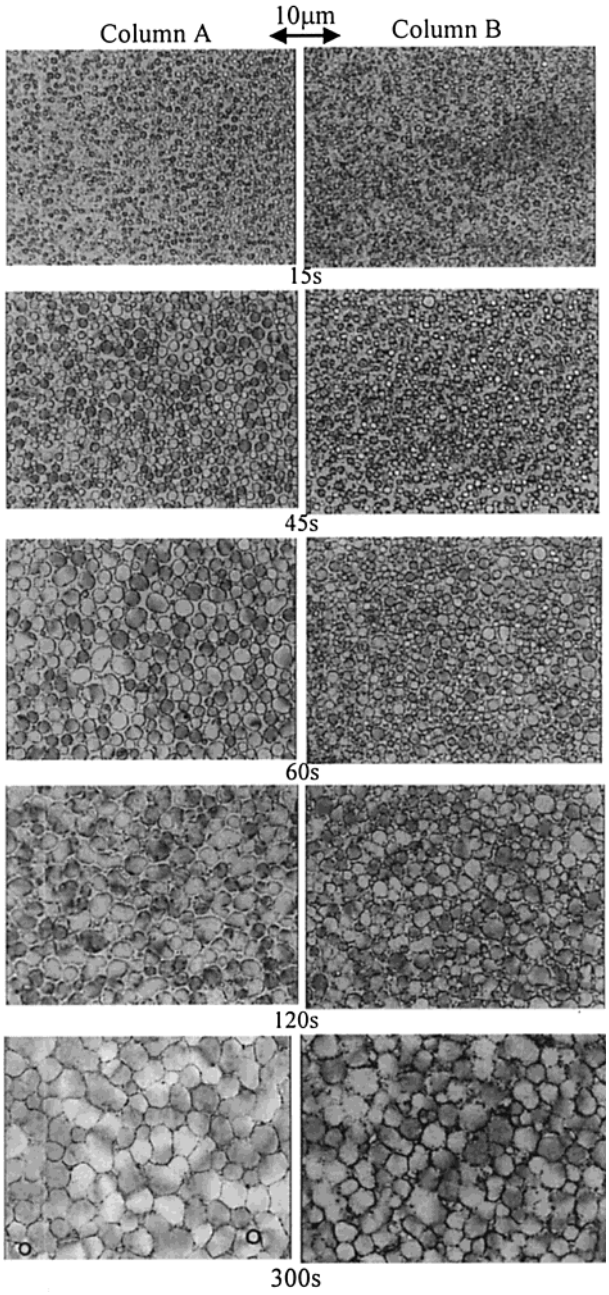

Figure 6. Comparison of temporal evolution of morphology of the 95/5 K21/NOA65 mixture photopolymerized under two conditions. Column A depicts the emergence of morphology of a single specimen subjected to photopolymerization, while column B shows the emergence of morphology of the fresh specimens subjected to photopolymerization at indicated times. Photoinitiation was undertaken in the single phase at 40 °C.

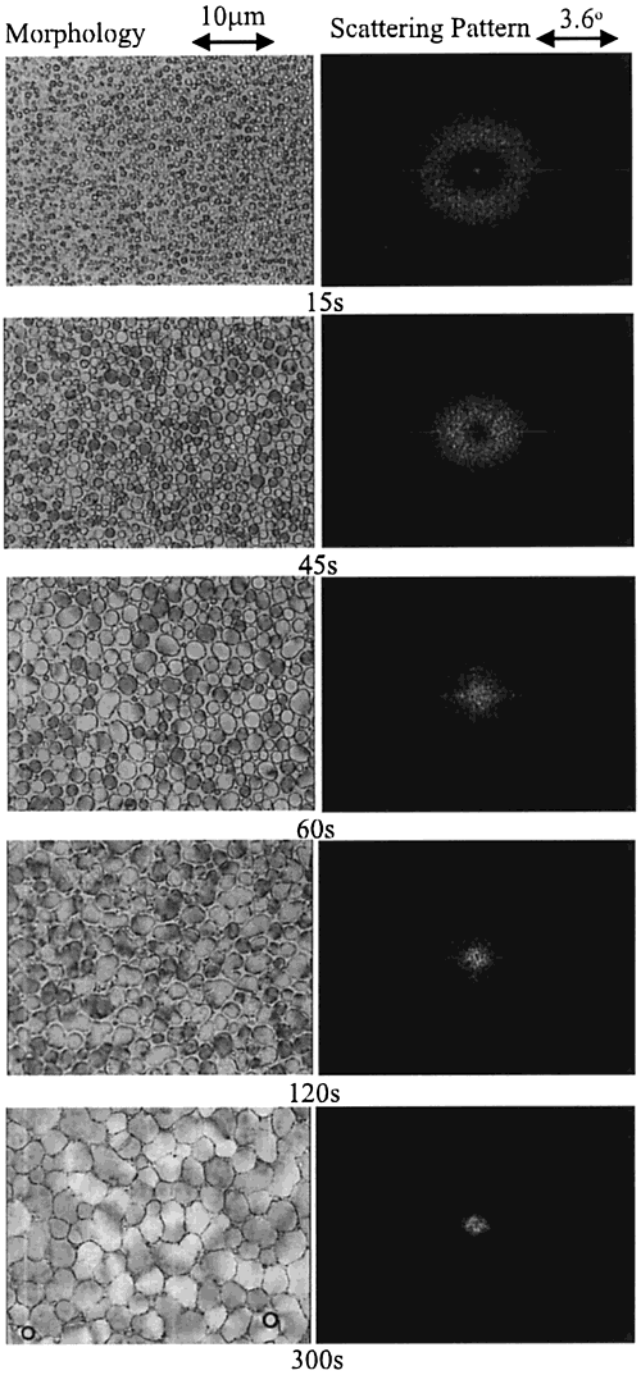

Figure 7. Temporal evolution of the domain morphology and the corresponding scattering patterns for the 95/5 K21/NOA65 mixture acquired during photopolymerization in the isotropic phase at 40 °C.

spinodal decomposition was found to shift to a lower angle while becoming more diffuse. The movement of the scattering peak is due to the domain growth. Since the 50/50 blend contains more monomer (NOA65), it is therefore more reactive than the 95/5 blend. Photopolymerization-induced phase separation is expected to occur faster in a mixture with a higher NOA65 concentration.

In the case of the 30/70 K15/NOA65 as depicted in Figure 8 (column B), the reaction is even much faster, thereby arresting the growth of the domains quickly and resulting in a finer morphology. Although the 30/70 blend corresponds to the off-critical mixture, the domains are seemingly interconnected, suggesting that the

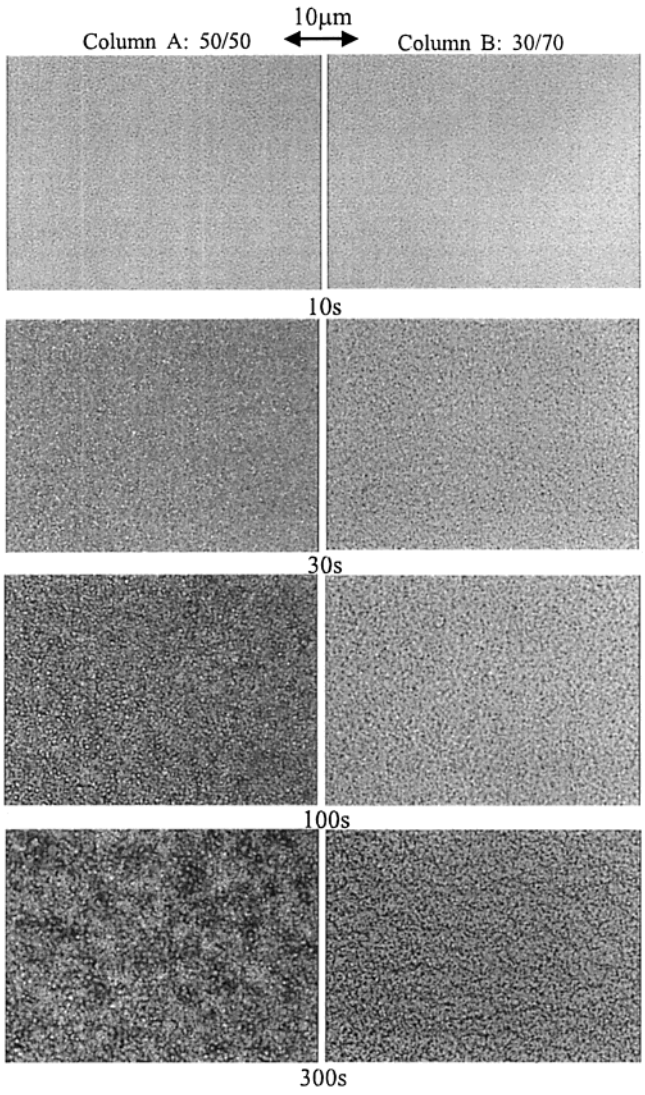

Figure 8. Time evolution of the domain morphology for (a) the 50/50 and (b) the 70/30 K21/NOA65 mixture. Photopolymerization was initiated in the isotropic phase at 40 °C. UV intensity was 40 mW/cm^2.

process of PIPS has probably advanced well into the unstable region where spinodal decomposition is dominant. With continued irradiation of the mixtures up to 300 s, the morphology does not change significantly as it is fixed by virtue of the formation of polymer network.

To quantify the growth dynamics, we examined the structure factors obtained from the 2D-FFT of the phase-separated structures acquired at different exposure times. Figure 9 shows the change of scattering curves as a function of irradiation time for the 95/5 K21/NOA65 mixture. It is seen that scattering peaks appeared within few seconds of photoinitiation. The scattering maximum shifts to a smaller wavenumber as time elapses, indicative of growth through coalescence in which larger domains grow at the expense of smaller ones. It is apparent that there is no linear regime corresponding to the early stage of phase separation (TIPS). The early stage of SD is generally characterized by the invariance of the scattering maximum with time for a brief period typically observed in some thermal quenched systems. On the other hand, the crossover from nucleation and growth to the spinodal decomposition characterizes the early stage of reaction-induced phase separation because of the asymmetric movement

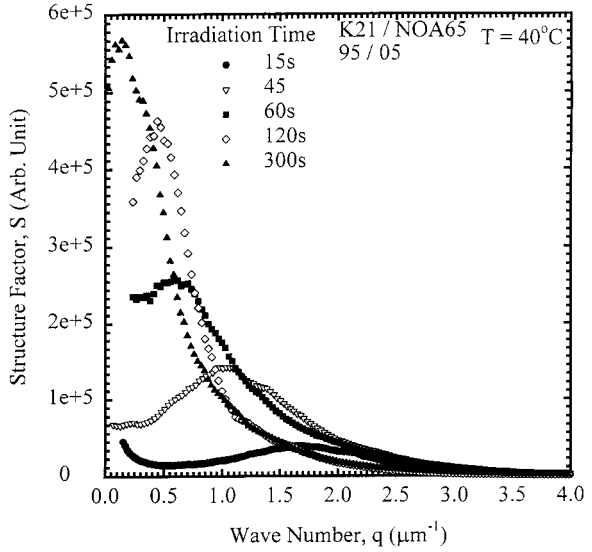

Figure 9. Temporal evolution of scattering profiles for various irradiation times, *t*, for the 95/5 K21/NOA65 mixture. Photopolymerization was initiated in the isotropic phase at 40 °C.

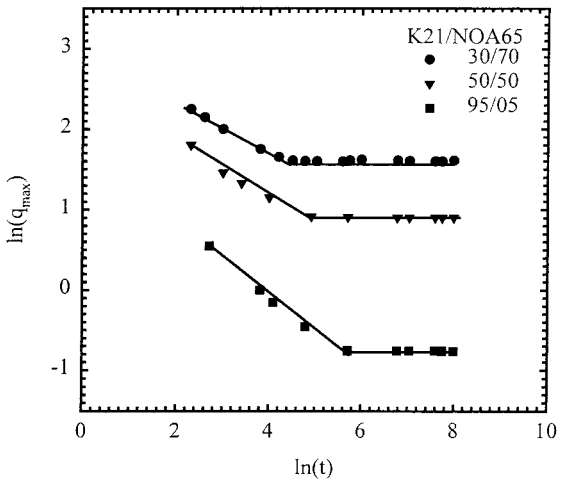

Figure 10. log−log plots of wavenumber maximum, q_{max}, versus irradiation time, *t*, for various blends subjected to photopolymerization in the single phase at 40 °C.

of the coexistence curve with reaction. This makes the system to fall into the metastable region before entering into the unstable region. The progressive movement of the coexistence curve makes the supercooling larger; therefore the domains tend to become smaller. The tendency of affording a small domain size is one of the unique characteristics of PIPS, but it is usually in competition with the domain growth associated with thermal relaxation. In the present case of photopolymerization-induced phase separation, the latter process prevails such that the coarsening takes place. It should be emphasized that the PIPS reaction is so fast that the coarsening process is seemingly completed within a short time interval, progressing rapidly into the unstable region where coarsening associated with thermal relaxation is expected to dominate.

We further analyze the growth dynamics in the context of the familiar power law scaling of the form $q_{max} = t^{-\alpha}$. Figure 10 shows the maximum wavenumber q_{max} versus irradiation time for the cured 30/70, 50/50, and 95/5 K21/NOA65 mixtures. The growth occurs rather rapidly in all compositions for some periods, and then the domains cease to grow when cross-linking takes place. It can be noticed that the cessation of growth occurs faster in the compositions high in reactive monomers in the sequence of 30/70, 50/50, and 95/5. This observation is not surprising in view of the fact that the mixtures with a higher NOA65 content would be more reactive, thereby arresting the domain growth earlier. This is exactly what one observes in the present study. It was found that the values of the kinetic exponent α range from approximately 0.32 for the 30/70 and 50/50 blends to 0.44 for the 95/5 K21/NOA65 blend. In view of the short time interval of growth, the observed exponents of 0.32 to 0.44 should not be overly interpreted, although these values are certainly within the range reported for the intermediate to late stages of spinodal decomposition in thermal quenched systems[41,46,50,51] and also in thermally initiated PIPS.[54] It should be pointed out that there is little or no difference of the growth exponent for the 30/70 blend (off-critical) and the 50/50 blend (critical for the starting K21/NOA65 monomer mixture). The observed similarity in the growth behavior in these two blends may be attributed to the movements of the critical point to a higher LC volume fraction during photopolymerization. This makes the 50/50 mixture to be off-critical, and thus it appear no different than the 30/70 mixture. A slightly larger growth exponent for the 95/5 K21/NOA65 mixture may be attributed to the high mobility of the LC molecules and the low viscosity associated with nematic ordering.

Concluding Remarks

In this work, we have demonstrated that the phase diagram of mixtures of nematic LC and reactive monomer is of the UCST type overlapping with the nematic−isotropic transition of the LC. It displayed isotropic liquid, isotropic liquid + isotropic liquid, isotropic liquid + nematic, and pure nematic coexistence regions. Both cross-linking polymerization and linear polymerization lead to a widening of the two-phase isotropic liquid + nematic (I + N) envelope of the phase diagram. There is no critical temperature associated with the LC/cross-linked polymer network phase diagram in comparison with that LC/linear polymer. Instead, the LC/cross-linked polymer phase diagram showed an upward turn in curvature as LC volume fraction approaches unity. The reason for this observed behavior is due to the domination of the elastic free energy of the cross-linked polymer network. Photopolymerization initiated in the isotropic phase resulted in uniformly distributed polygonal-shaped LC droplets in contrast to photopolymerization initiated in the two-phase region. Of particular interest is that the size of phase-separated LC droplets increases with increasing LC concentration. The network morphology is reminiscent of interconnected threads seemingly running through the interstices of the polygonal droplets. Despite the short time interval for the domain growth due to the fast curing, the growth exponent of approximately $^1/_3$ was observed in the PIPS dynamics studies. The growth is seemingly expedited in the high LC (95%) blend due to the slower curing of the NOA65 in such a high LC concentration such that the structural growth due to thermal relaxation would prevail as the mobility of LC molecules would be high, and the viscosity is expected to reduce because of the nematic ordering.

Acknowledgment. Support of this work by the NSF-STC Center for Advanced Liquid Crystal Optical Materials (ALCOM) via Grant 89-20147 is gratefully acknowledged.

References and Notes

(1) Drzaic, P. S. *Liquid Crystal Dispersion*; World Scientific: Singapore, 1995.
(2) Doane, J. W. In *Liquid Crystals: Applications and Uses*; Bahadur, B., Ed.; World Scientific: Singapore, 1991.
(3) Montgomery, G. P.; Smith, G. W.; Vaz, N. A. In *Liquid Crystalline and Mesomorphic Polymers*; Shibaev, V. P., Lam, L., Eds.; Springer: New York, 1994.
(4) Yang, D.-K.; Chien, L.-C.; Fung, Y. K. In *Liquid Crystals in Complex Geometry Formed by Polymer and Porous Networks*; Crawford, G. P., Zumer, S., Eds.; Taylor & Francis: London, 1996.
(5) Doane, J. W.; Golemme, A.; West, J. L.; Whitehead, J. B.; Wu, B.-G. *Mol. Cryst. Liq. Cryst.* **1988**, *165*, 511.
(6) Braun, D.; Frick, G.; Grell, M.; Klines, M.; Wendorff, J. H. *Liq. Cryst.* **1992**, *11*, 929.
(7) Yamaguchi, R.; Sato, S. *Liq. Cryst.* **1993**, *14*, 929.
(8) Lovinger, A. J.; Amundson, K. R.; Davis, D. D. *Chem. Mater.* **1994**, *6*, 1726.
(9) Yang, D.-K.; Chien, L.-C.; Doane, J. W. *Appl. Phys. Lett.* **1992**, *60*, 25.
(10) Rajaram, C. V.; Hudson, S. D.; Chien, L. C. *Chem. Mater.* **1995**, *7*, 2300.
(11) Rajaram, C. V.; Hudson, S. D.; Chien, L. C. *Chem. Mater.* **1996**, *8*, 2451.
(12) Doane, J. W.; Yang, D.-K.; Yaniv, Z. *Proc. SID Japan Display* **1992**, 73.
(13) Serbutoviez, C.; Kloosterboer, J. G.; Boots, H. M. J.; Touwslager, F. J. *Macromolecules* **1996**, *29*, 7690.
(14) Molsen, H.; Kitzerow, H.-S. *J. Appl. Phys.* **1994**, *75*, 710.
(15) Kitzerow, H.-S.; Molsen, H.; Heppke, G. *Appl. Phys. Lett.* **1992**, *60*, 3093.
(16) Lee, K.; Suh, S.-W.; Lee, S.-D. *Appl. Phys. Lett.* **1994**, *64*, 718.
(17) Dumon, M.; Nguyen, H. T. *Polym. Adv. Technol.* **1992**, *3*, 197.
(18) Lester, G.; Cotes, H.; Murayama, A.; Ishikawa, M. *Ferroelectrics* **1993**, *148*, 389.
(19) Guymon, C. A.; Hoggan, E. N.; Walba, D. M.; Clark, N. A.; Bowman, C. N. *Liq. Cryst.* **1995**, *19*, 719.
(20) Guymon, C. A.; Hoggan, E. N.; Rieker, T. P.; Clark, N. A.; Walba, D. M.; Bowman, C. N. *Science* **1997**, *275*, 57.
(21) Clark, N. A.; Lagerwall, S. T. *Appl. Phys. Lett.* **1980**, *36*, 899.
(22) Walba, D. M. *Science* **1995**, *270*, 250.
(23) Guymon, C. A.; Bowman, C. N. *Macromolecules* **1997**, *30*, 1594; **1997**, *30* 5271.
(24) Hikmet, R. A. M.; Lub, J.; Maasen vd Brink, P. *Macromolecules* **1992**, *25*, 4194.
(25) Hikmet, R. A. M. *J. Appl. Phys.* **1990**, *68*, 4406.
(26) Hikmet, R. A. M.; Zwerver, B. H. *Liq. Cryst.* **1991**, *10*, 835.
(27) Hirai, R.; Niiyama, S.; Kumai, H.; Gunjima, T. *Proc. SPIE-Int. Soc. Opt. Eng.* **1990**, *1257*, 2; *Rep. Res. Lab., Asahi Glass Co., Ltd.* **1990**, *40*, 285.
(28) Nolan, P.; Tillin, M.; Coates, D. *Mol. Cryst. Liq. Cryst. Lett.* **1992**, *8*, 129.
(29) LeGrange, J. D.; Miller, T. M.; Wiltzius, P.; Amundson, K. J.; Boo, J.; van Blaaderen, A.; Srinivasarao, M.; Kmetz, A. *SID Digest* **1995**, *193*, 275.
(30) Nwabunma, D.; Kim, K.-J.; Lin, Y.; Chien, L.-C.; Kyu, T. *Macromolecules* **1998**, *31*, 6806.
(31) Nwabunma, D.; Kyu, T. *Macromolecules* **1999**, *32*, 664.
(32) Technical Data Sheet for NOA65 Optical Adhesive, Norland Products, Inc., New Brunswick, NJ.
(33) Smith, G. W. *Mol. Cryst. Liq. Cryst.* **1991**, *196*, 89.
(34) Shen, C.; Kyu, T. *J. Chem. Phys.* **1995**, *102*, 556.
(35) Shen, C. Ph.D. Dissertation, The University of Akron, 1995.
(36) Flory, P. J. *J. Chem. Phys.* **1942**, *10*, 51.
(37) Huggins, M. L. *J. Chem. Phys.* **1941**, *9*, 440.
(38) Maier, W.; Saupe, A. *Naturforsch* **1958**, *A13*, 564; **1959**, *A14*, 882; **1960**, *A15*, 287.
(39) Smith, G. W. *Int. J. Mod. Phys. B* **1993**, *7*, 4187.
(40) Kim, W.-K.; Kyu, T. *Mol. Cryst. Liq. Cryst.* **1994**, *250*, 131.
(41) Kyu, T.; Ilies, I.; Shen, C.; Zhou, Z. L. In *Liquid Crystalline Polymer Systems: Technological Advances*; Isayev, A., Kyu, T., Cheng, S. Z. D., Eds.; ACS Symp. Ser. 632; American Chemical Society: Washington, DC, 1996.
(42) West, J. L. *Mol. Cryst. Liq. Cryst.* **1988**, *157*, 427.
(43) Ahn, W.; Kim, C. Y.; Kim, H.; Kim, S. C. *Macromolecules* **1992**, *25*, 5002.
(44) Pracella, M.; Bresci, B.; Nicolardi, C. *Liq. Cryst.* **1993**, *14*, 881.
(45) Dorgan, J. R.; Soane, D. S. *Mol. Cryst. Liq. Cryst.* **1990**, *188*, 129.
(46) Kyu, T.; Ilies, I.; Mustafa, M. *J. Phys. IV* **1993**, *3*, 37.
(47) Russel, G. M.; Paterson, B. J. A.; Imrie, C. T. *Chem. Mater.* **1995**, *7*, 2185.
(48) Amundson, K.; van Blaaderen, A.; Wiltzius, P. *Phys. Rev. E* **1997**, *55*, 1646.
(49) Chien, L.-C.; Boyden, M. N.; Walz, A. J.; Citano, C. M. In ref 41.
(50) Chiu, H.-W.; Zhou, Z. L.; Kyu, T.; Cada, L. G.; Chien, L.-C. *Macromolecules* **1996**, *29*, 1051.
(51) Mukherjee, P.; Kyu, T. *Liq. Cryst.* **1988**, *3*, 631.
(52) Lin, Z.; Zhang, H.; Yang, Y. *Macromol. Chem. Phys.* **1999**, *200*, 943.
(53) Kim. J. Y.; Palffy-Mulhoray, P. *Mol. Cryst. Liq. Cryst.* **1991**, *203*, 93.
(54) Kim. J. Y.; Cho, C. H.; Palffy-Mulhoray, P.; Mustafa, M.; Kyu, T. *Phys. Rev. Lett.* **1993**, *71*, 2232.
(55) Srinivasarao, M.; Amundson, K. *Polym. Prepr. (Am. Chem. Soc., Div. Polym. Chem.)* **1996**, *37*, 200.

MA9912296